ELSEVIER

Materials Science and Engineering B30 (1995) 127–136

MATERIALS SCIENCE & ENGINEERING B

Structure and formation energy of steps on the GaAs(001)-2 × 4 surface

S.B. Zhang, Alex Zunger

National Renewable Energy Laboratory, Golden, CO 80401, USA

Abstract

The energies of various steps on the As-terminated GaAs(001)-2 × 4 surface are evaluated using a novel, approximate method of "linear combination of structural motifs". It is based on the observation that previous total energy minimizations of semiconductor surfaces produced invariably equilibrium structures made of the same recurring local structural motifs, e.g. tetrahedral fourfold Ga, pyramidal threefold As, etc. Furthermore, such surface structures were found to obey consistently the octet rules as applied to the local motifs. We thus express the total energy of a given semiconductor surface as a sum of (i) the energies $\{\varepsilon_M\}$ of the local structural motifs appearing in the surface under consideration and (ii) an electrostatic term representing the Madelung energy of point charges resulting from application of the octet rule. The motif energies are derived from a set of pseudopotential total energy calculations for flat GaAs(001) surfaces and for point defects in bulk GaAs. This set of parameters suffices to reproduce the energies of other (001) surfaces, calculated using the same pseudopotential total energy approach. Application to GaAs(001)-2 × 4 surfaces with steps reveals the following. (i) "Primitive steps", defined solely according to their geometries (i.e. step heights, widths and orientations) are often unstable. (ii) Additional, non-geometric factors beyond step geometries such as addition of surface adatoms, creation of vacancies and atomic rebonding at step edges are important to lower step energies. So is step–step interaction. (iii) The formation of steps is generally endothermic. (iv) The formation of steps with edges parallel to the direction of surface As dimers (A steps) is energetically favored over the formation of steps whose edges are perpendicular to the As dimers (B steps).

Keywords: Surface energy; Total binding energy; Surface structure; Gallium arsenide

1. Introduction

Surface steps carry the two-dimensional (2D) surface physics into the domain of one-dimensional (1D) structures. Such steps are potentially important in (i) step flow growth controlling the quality of thin films, (ii) the fabrication of artificial lateral superlattices using vicinal surfaces [1], and (iii) control of spontaneous ordering and the ensuing band gap engineering in semiconductor alloys [2].

Questions regarding GaAs(001) surface steps range from the nature of their equilibrium shapes and micron scale morphologies to the atomic scale structures of steps, from thermoequilibrium properties of steps to step dynamics during growth. Recent experimental studies on GaAs(001) surface steps include (i) the scanning tunneling microscopy study on surface topologies and island structures by Pashley et al. [3], (ii) the stability analysis of GaAs(001) homoepitaxy growth by Johnson et al. [4], (iii) the measurement of step and kink energies by Heller et al. [5], (iv) the observation of step bunching and step meandering [6], and (v) the effects of growth interruption and subsequent surface annealing [7], all on molecular beam epitaxy (MBE) grown samples with 2 × 4 surface reconstruction, and in addition (vi) the observation of multilayer steps [8] on samples grown by metal organic chemical vapor deposition. Previous theoretical investigations on GaAs(001) surface steps focused largely on the growth kinetics which provides the time evolution sequence for various growth processes, step motion and surface diffusion [9–11]. To date, little is known on the atomic structure of GaAs(001) steps. Here, we present a theoretical study of the energetics of various step structures on GaAs(001)-2 × 4 surfaces. We developed a simple approach that predicts step energies based on a small number of local density approximation (LDA) total energy calculations on flat surfaces and bulk point defects. Steps are then examined in terms of (i) step geometries (heights, widths, orientations etc.) and (ii)

SSDI 0921-5107(94)09007-6

"electronic additions" (i.e. surface adatoms or vacancies) that lead to electronic compensation and thus to stable and semiconducting flat surfaces. While step–step interaction has noticeable effects on step formation energies, the formation of steps is generally endothermic. There are two commonly observed steps: those with edges parallel to the direction of surface As dimers (A steps) and those whose edges are perpendicualr to the As dimers (B steps).

The calculated ratio of formation energies of the A to B steps is 3–6, suggesting that A steps are more abundant than B steps.

2. Theory: linear combination of structural motifs

While it is possible to calculate directly from first principles the total energies of various flat surface structures [12–14], and to some degree the relative energies of different step structures [15], these types of calculations suggest a simpler, approximate approach. In fact, in a relatively large collection of (001) surface structure calculations [12–14], as well as in calculated bulk point defect structures [16], the Ga and As atoms assume only a limited number of local structures to be named here "structural motifs". Using the superscript (i) to denote the coordination number, the structural motifs include (Fig. 1) tetrahedrally bonded $Ga^{(4)}$ and $As^{(4)}$, pyramidal $As^{(3)}$, planar $Ga^{(3)}$, and bridge site $Ga^{(2)}$, with bond angles of 109.5°, 90°, 120°, and 180° respectively. A close examination of the actual atomic structures indicates that deviations from these ideal angles are usually in the range of $\pm 10°$. In addition to the one-site motifs, Fig. 1 also shows some two-site 'wrong bond" motifs (e.g. the Ga–Ga and As–As bonds).

Previous studies of GaAs(001) surfaces [17] revealed that the octet rule tends to be obeyed by these motifs, leading to a set of point charges on various surface atoms. For example, Ga has 3 valence electrons, so fourfold coordinated $Ga^{(4)}$ contributes 3/4 electrons to each of its four bonds. This leads to local charge neutrality. Planar $Ga^{(3)}$ is a 3/4 electron donor as it tends to empty its dangling bond level (located near the conduction band minimum (CBM)) so as to satisfy locally the octet rule (see Fig. 1). Similarly, while fourfold coordinated $As^{(4)}$ is neutral, with 5/4 electrons in each of its four bonds, pyramidal $As^{(3)}$ is a $2-5/4=3/4$ electron acceptor since it needs to acquire this many electrons to fill completely its dangling bond level (located near the valence band maximum). We see that the assignment of a $+3/4$ charge to $Ga^{(3)}$ and of a $-3/4$ charge to $As^{(3)}$ ensures that the gap states are completely full or completely empty so that the systems remain semiconducting. This octet shell (fully occupied or fully empty levels) is necessary, but not sufficient, to create a low energy state. In fact, by combining the $Ga^{(3)}$ with the $As^{(3)}$ we can achieve charge neutrality through charge compensation, thus gaining the energy resulting from charge transfer from the $Ga^{(3)}$ donor level to the $As^{(3)}$ acceptor level (approximately 3/4 of the energy gap). Total energy calculations indeed tend to produce surface structures that reflect such charge compensations [13,14]. Recently, it was further demonstrated [14] that such a charge compensation–electron counting model can be used in a quantitative fashion to explain the order of surface energies in flat GaAs(001) surfaces with identical surface motifs.

Based on the existence of recurring surface structural motifs and the adherence to the octet rule, we postulate that the formation energy of a system σ of defects, surfaces or steps, due to chemical reaction, i.e.

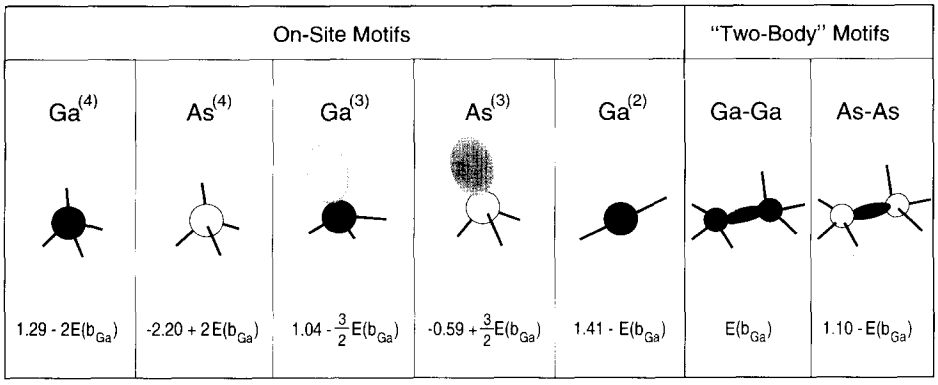

Fig. 1. Structural motifs are depicted in a ball and stick model together with the motif energies. Both the empty and filled dangling bond orbitals of $Ga^{(3)}$ and $As^{(3)}$ and the Ga–Ga and As–As "wrong bonds" are shaded. b_{Ga} and b_{As} denote "Ga–Ga" and "As–As" respectively.

$\sigma_0 \rightarrow \sigma$ (we use as reference for Eq. (1) bulk GaAs for defects, the $\alpha(2\times4)$ surface for flat surfaces and $\beta2(2\times4)$ surface for stepped surfaces), can be written as

$$\Delta E(\sigma, \mu_R) = \Delta E_{LCSM}(\sigma) + \Delta E_{Mad}(\sigma) + \Sigma \mu_R N_R \quad (1)$$

where

$$E_{LCSM}(\sigma) = \sum_M \omega_M(\sigma)\varepsilon_M \quad (2)$$

is a linear combination of structural motif (LCSM) energies ε_M with ω_M being the frequency of occurrence of motif M in the structure σ. The second term in Eq. (1) is the electrostatic energy:

$$E_{Mad}(\sigma) = \frac{1}{2\varepsilon} \sum_{i,j}{}' \frac{q_i q_j}{|R_i - R_j|} \quad (3)$$

where q_i is the charge of the ith motif at position R_i resulting from adherence to the octet rule and ε is the effective dielectric constant. We assume that stable and close to stable surface structures must combine donor and acceptor states so as to become (by the octet rule) charge neutral, $\Sigma_i q_i = 0$. The last term in Eq. (1), $\Sigma \mu_R N_R$, accounts for particle exchange with reservoir R, containing Ga and As with chemical potentials μ_{Ga} and μ_{As}, and free electrons with a Fermi energy μ_e (i.e. R = (Ga, As, free electron) and $\mu_R = (\mu_{Ga}, \mu_{As}, \mu_e)$). N_R are the net particle exchanges during the reaction. For example, formation of a Ga vacancy in bulk GaAs leads to the capture of 3 electrons from the "Fermi sea" and to the ejection of a Ga atom into the Ga reservoir. The formal reaction is

$$3e^- + Ga_{Ga}{}^0 \rightarrow V_{Ga}{}^{3-} + Ga \text{ (at reservoir)} \quad (4)$$

Thus, the change in total energy in this reaction is

$$\Delta E = E(V_{Ga}{}^{3-}) + \mu_{Ga} - 3\mu_e \quad (5)$$

so $N_{Ga} = 1$ and $N_e = -3$. We also assume that the system σ is in equilibrium with bulk GaAs. This leads to the constraint that

$$\mu_{Ga} + \mu_{As} = \mu_{GaAs} = -\Delta H \quad (6)$$

where $\Delta H = 0.92$ eV [13] is the heat of formation of bulk GaAs. Note that we thus envision the case where a GaAs surface or bulk defect exists in equilibrium with a reservoir containing Ga, As and solid GaAs. The permissible events are deposition of solid Ga (if μ_{Ga} exceeds μ_{Ga}(solid Ga)), deposition of solid As (if μ_{As} exceeds μ_{As}(solid As)), formation of bulk GaAs, or formation of a particular surface or defect structure σ. All other reactions are assumed to be of higher energy, hence irrelevant. Eq. (6) allows us to eliminate a single variable, i.e. μ_{As}, and to express the formation energy as $\Delta E(\sigma, \mu_{Ga}, \mu_e)$. The range of the chemical potential μ_{Ga} is bound by the formation of solid Ga and solid As. This leads to $-\Delta H \le \mu_{Ga} \le 0$. The range of the Fermi energy is bound by the band gap of GaAs, i.e. $0 \le \mu_e \le E_g = 1.5$ eV (see Ref. [16]). Since we use explicitly the charge compensation–electron counting model, the surface and step formation energies are independent of μ_e, i.e. $\Delta E = \Delta E(\sigma, \mu_{Ga})$.

We will extract the energies ε_M of the local motifs by fitting Eq. (1) to a set of LDA calculations on point defects and on flat surfaces. The reliability of the LCSM approach will then be tested by its ability to reproduce LDA energies of independently calculated surface structures.

The coefficients ω_M of the various motif energies and the coefficients N_R of the chemical potential terms are listed in Table 1 for various defects and (001) surface structures discussed in this paper. Results of the ab initio LDA calculation are given in the last column. Seven LDA energies are then used to deduce the motif energies ε_M by equating the LCSM energy of Eq. (1) to the LDA energy. The other ten LDA total energies (Table 1) are used to test the LCSM. In deriving the motif energies, we first combine the four point defect energies of bulk GaAs (rows 1–4 in Table 1) with Eq. (6). This leads to five motif energies $\varepsilon(Ga^{(4)})$, $\varepsilon(As^{(4)})$, $\varepsilon(Ga^{(3)})$, $\varepsilon(As^{(3)})$, and ε(As–As), all expressed in terms of ε(Ga–Ga). These are given in Fig. 1 (since we are only dealing with systems with particle conservation, there is no need to determine the absolute value of motif energies). Second, we used three surface structures ($\beta2(4\times2)$, $c(8\times2)$ and $c(2\times2)$; see rows 11, 12 and 16 in Table 1) to determine the remaining motif energy parameters $\delta\varepsilon$(As–As) and $\varepsilon(Ga^{(2)})$, and the effective surface dielectric constant ε_s appearing in E_{Mad}. We obtain $\delta\varepsilon$(As–As) = −0.45 eV, which reflects the strengthening of the As–As bond by formation of surface As–As dimers, and $\varepsilon_s = 8.1$. One may independently derive the surface dielectric constant ε_s from classical electrodynamics [18] using a GaAs bulk dielectric constant of 13. The result is $\varepsilon_s = 7$, in reasonable agreement with our fitted result of 8.1.

Having established the energies $\{\varepsilon_M\}$ of the characteristic motifs and the effective dielectric constant ε_s, we can now use Eq. (1) to predict the energies of independent surface structures. Comparison of the LCSM results with LDA results for structures not used in the fit (see entries in Table 1 not marked "fitted") shows that the LCSM calculation is accurate to within 0.1 eV per (1×1).

3. Steps on vicinal GaAs(001)-2 × 4 surfaces

We now examine steps on vicinal GaAs(001)-2 × 4 surfaces. A $\beta2(2\times4)$ structure is assumed here since,

Table 1
Coefficients $\omega_M(\sigma)$ denoting the frequency of motif M, coefficients N_R of the chemical potential terms in structure σ for (i) point defects, (ii) (001) surfaces and (iii) (001) − 2 × 4 surface steps of GaAs and appropriate energies

	$\omega_M(\sigma)$ for the following								N_R for the following					
	$Ga^{(4)}$	$As^{(4)}$	$Ga^{(3)}$	$As^{(3)}$	$Ga^{(2)}$	Ga–Ga	As–As	δ_{As-As}	μ_{e4}	μ_{Ga}	ΔH	ΔE_{Mad} (eV)	ΔE (eV)	ΔE^*_{LDA} (eV)
(i) Defects (per defect)														
(1) V_{Ga}^{3-}	−1	−4	0	4	0	0	0	—	3	1	0	0.52	Fitted	5.78
(2) V_{As}^{3+}	−4	−1	4	0	0	0	0	—	3	−1	−1	0.52	Fitted	0.77
(3) Ga_{As}^{2-}	1	−1	0	0	0	0	0	—	−2	−2	−1	0	Fitted	2.45
(4) As_{Ga}^{2+}	−1	1	0	0	0	0	4	—	2	2	1	0	Fitted	1.98
(ii) Surfaces (per 1 × 1)														
(5) $\alpha(2\times4)$	0	0	0	0	0	0	0	0	0	0	0	0	0	0
(6) $\alpha(4\times2)$	0	0	0	0	0	0	0	−1/4	0	0	0	$0.04/\varepsilon_s$	0.12	0.12
(7) $\beta(2\times4)$	0	0	0	1/4	0	−1/4	1/8	1/8	0	1/4	1/4	$-0.22/\varepsilon_s$	$0.14+(1/4)\mu_{Ga}$	0.07
(8) $\beta2(2\times4)$	0	0	0	1/4	0	−1/4	1/8	1/8	0	1/4	1/4	$-0.80/\varepsilon_s$	$0.06+(1/4)\mu_{Ga}$	0.02
(9) $\beta(4\times2)$	0	0	1/4	0	0	1/8	−1/4	−1/4	0	−1/4	0	$0.01/\varepsilon_s$	$0.09-(1/4)\mu_{Ga}$	0.00
(10) $\beta_{rep}(4\times2)$	0	0	3/8	−1/8	0	1/2	−1/4	−1/4	0	−1/2	−1/8	$0.05/\varepsilon_s$	$0.18-(1/2)\mu_{Ga}$	0.08
(11) $\beta2(4\times2)$	0	0	1/4	0	0	1/8	−1/4	−1/4	0	−1/4	0	$-0.87/\varepsilon_s$	Fitted	−0.03
(12) $c(8\times2)$	0	0	0	0	0	0	0	0	0	0	0	$0.89/\varepsilon_s$	Fitted	0.12
(13) $\gamma(2\times4)$	0	0	0	1/2	0	−1/4	1/2	1/2	0	1/2	1/2	$-1.20/\varepsilon_s$	$0.34+(1/2)\mu_{Ga}$	0.32
(14) $c(4\times4)$	0	0	−1/2	3/4	0	−1/4	13/8	13/8	0	5/4	3/4	$-0.43/\varepsilon_s$	$0.73+(5/4)\mu_{Ga}$	0.69
(15) 2 × 1	1/2	0	−1/2	1/2	1/2	−1/4	−1/4	−1/4	0	0	1/2	$-5.51/\varepsilon_s$	0.15	0.07
(16) $c(2\times2)$	1/2	0	−1/2	1/2	1/2	−1/4	−1/4	−1/4	0	0	1/2	$-6.32/\varepsilon_s$	Fitted	0.05
(iii) Steps (per 1 ×)														
(17) BII-1-$\beta(2\times4)$	0	0	1/2	3/8	0	0	−3/16	−3/16	0	−1/8	3/8	$-3.55/\varepsilon_s$	$0.14-(1/8)\mu_{Ga}$	0.16
(18) Double A-$\beta2(2\times4)$	0	0	0	0	0	0	0	0	0	0	0	$0.43/\varepsilon_s$	0.05	0.05

ΔE_{Mad} is the Madelung energy, ΔE is the LCSM formation energy (for defects, surfaces, and steps), and $\Delta E^*_{LDA} = \Delta E_{LDA} - N_c\mu_c - N_{Ga}\mu_{Ga}$ the corresponding LDA formation energy. —, not applicable. A dielectric constant $\varepsilon_b = 13$ is used to calculate the Madelung energy for vacancies containing four point charges whereas $E_{Mad} = 0$ is used for single point charge antisites.

according to Refs. [13,14], this is the most stable 2×4 surface structure, covering the chemical potential range -0.7 eV$>\mu_{Ga}>-0.2$ eV. This surface has As–As dimers parallel to the $[1\bar{1}0]$ direction. Dimerization thus makes the two orthogonal [110] and $[1\bar{1}0]$ directions on this surface inequivalent. There are therefore two types of basic steps (A and B) on GaAs(001)-2×4 surfaces: the A step has edges along the $[1\bar{1}0]$ direction, whereas the B step has edges along the [110] direction. In the following, we will discuss step structures, step energetics, and the effects of kinks on step energies.

3.1. Primitive bilayer steps: unstable structures

Primitive steps are defined solely by their geometry, and not by any other measure such as the degree of electron compensation. We will consider here only bilayer height steps (see, however, Section 3.2) differing only in their width w_{step} normal to the step edges and in their orientation (i.e. A or B steps). A step width is irreducible if it is less than the dimension w_{surf} of the flat surface cell. Denoting by a_s the dimension of unreconstructed 1×1 surface cells, we have $a_s=a/\sqrt{2}$ where a is the bulk lattice constant. The condition $w_{step}<w_{surf}$ leads to four possible primitive bilayer height A steps AI, AII, AIII and AIV with $w_{step}=\frac{3}{2}a_s$, $\frac{5}{2}a_s$, $\frac{7}{2}a_s$ and $\frac{1}{2}a_s$, and two primitive bilayer height B steps BI and BII of $w_{step}=\frac{3}{2}a_s$ and $\frac{1}{2}a_s$ wide. Top and side views of the AI and AII steps are given in Fig. 2, while similar views of the BI and BII steps are given in Fig. 3. We do not show models for the AIII and AIV steps since our calculations show that they do not lead to stable step structures.

Charge assignments following the octet rule (shown in the lower halves of Figs. 2 and 3) indicate that none of the primitive steps here is charge neutral: if e denotes the absolute value of the electron charge, and $1\times$ denotes one step unit of length a_s along the step edge, then the AI and AII steps have a charge of $+0.25e/(1\times)$ and $-0.25e/(1\times)$ respectively, while the BI step has a charge of $+1.75e/(1\times)$ and the BII step has $-0.75e/(1\times)$. Since the electrostatic energy of an infinitely long 1D charge diverges, none of the primitive steps is stable. One can lower the energy of the primitive steps by restoring charge neutrality. This is illustrated next.

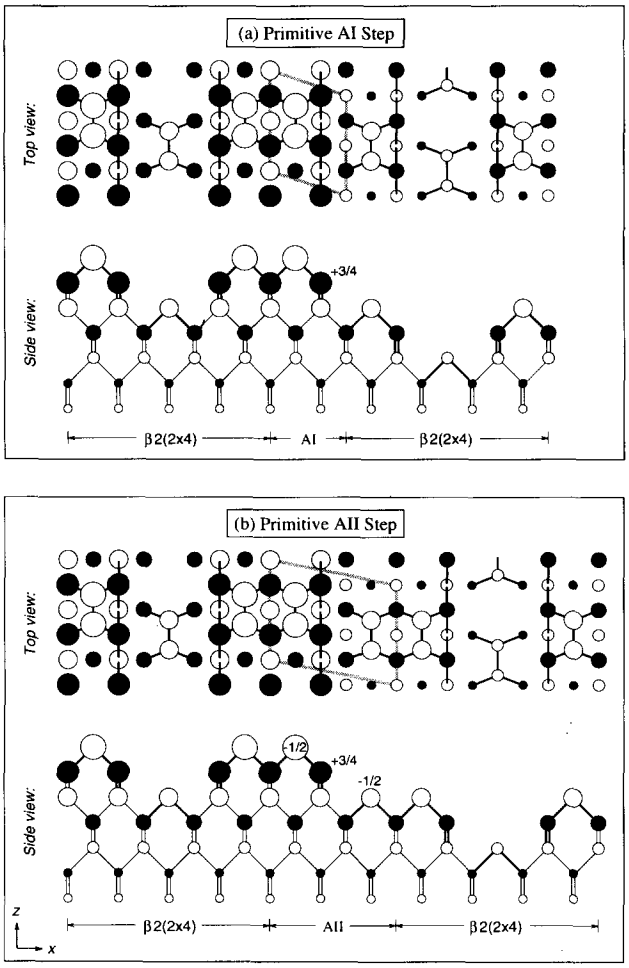

Fig. 2. Top and side views of the primitive (a) AI and (b) AII steps. The filled and open circles denote Ga and As respectively with descending sizes from the surface. The thick bonds in the side view indicate the surface bonds shown in the top view. The numbers in the side view indicate charge assignments according to the octet rule, and the thick line is the step unit cell. To illustrate how the step cell fits into a flat $\beta2(2\times4)$ surface, two complete $\beta2(2\times4)$ surface cells (one at the upper terrace and one at the lower terrace) are shown in the figure.

3.2. Charge compensated derivative steps

Derivative steps are derived through charge compensation of primitive steps. Figs. 4 and 5 show, for A-type and B-type primitive steps respectively, the lowest energy derivative steps as obtained from the LCSM study of about 30 step structures. These low energy derivative steps are locally charge compensated, i.e. compensation takes place essentially within the range of a 2×4 surface cell. According to our LCSM calculation, structures involving charge compensation beyond the scale set by the 2×4 cell are higher in energy and are thus not discussed here. Three distinct local charge compensation patterns are evident in Figs. 4 and 5.

(1) *Charge compensation by adatoms.* The simplest example here is the twofold $Ga^{(2)}$ adatom in Fig. 4(b) (AII-1). To form a bridge site $Ga^{(2)}$, one first needs to break one As–As dimer bond containing two electrons, and second one needs to insert the Ga thus

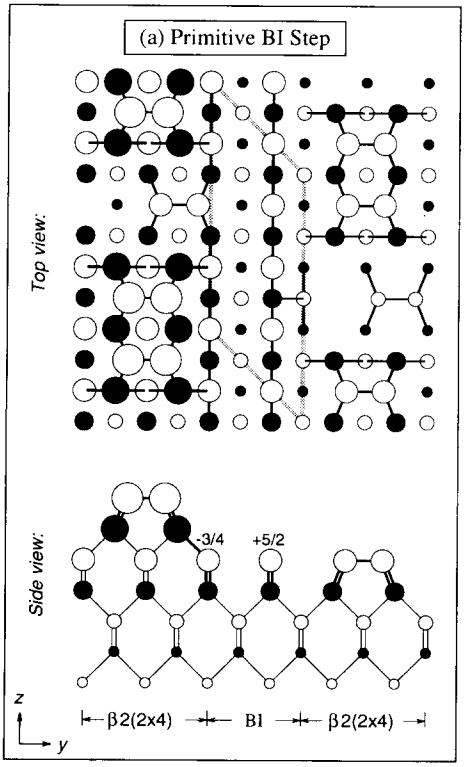

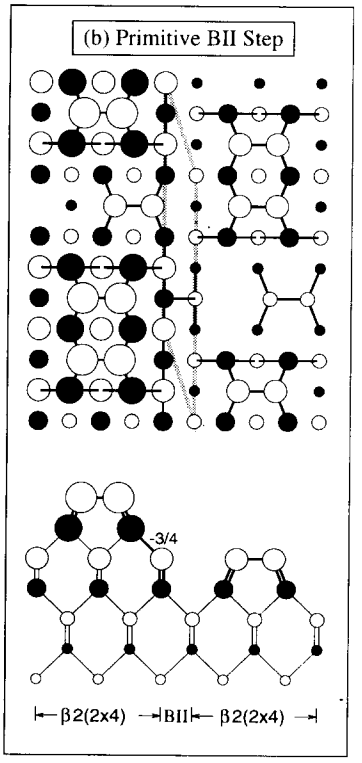

Fig. 3. Top and side views of the primitive (a) BI and (b) BII steps. Details as for Fig. 3.

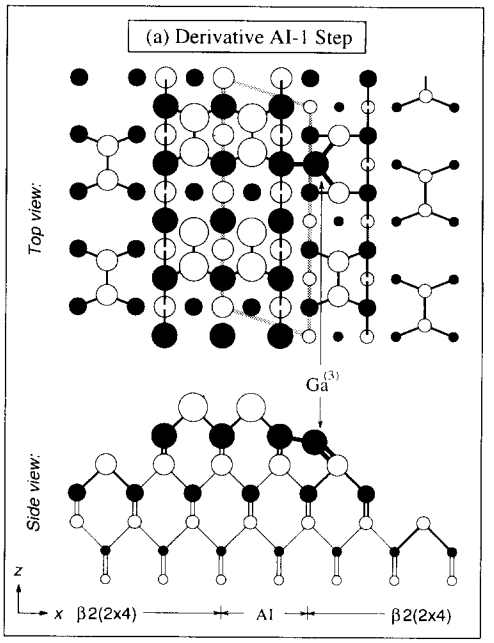

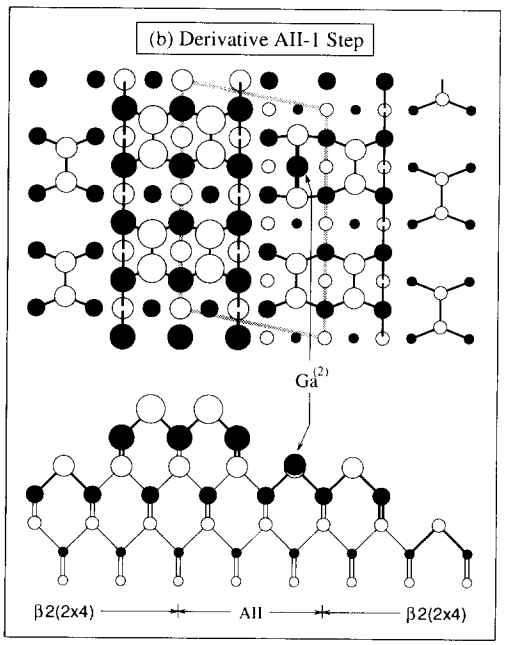

Fig. 4. Top and side views of the derivative (a) AI-1 and (b) AII-1 steps. The filled and open circles are Ga and As respectively, with descending sizes from the surface. The thick bonds in the side view indicate the surface bonds shown in the top view. The thick line is the step unit cell. Note that, unlike Fig. 2, only part of the flat $\beta 2(2\times 4)$ surface cells are shown here.

making two Ga–As bonds. When the As–As dimer bond is broken, each As is left with one electron. A $Ga^{(2)}$ thus contributes one electron to each of the two newly formed Ga–As bonds. Since Ga has a valence of 3 and the next available state of $Ga^{(2)}$ (as determined by LDA calculation) is near the CBM, the $Ga^{(2)}$ is a one

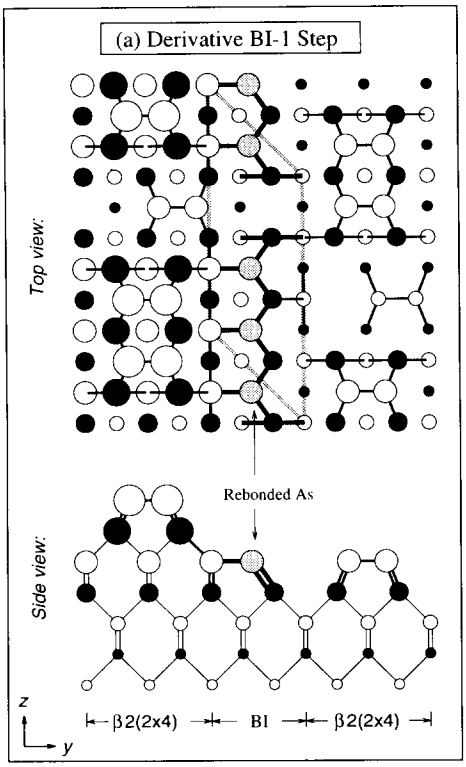

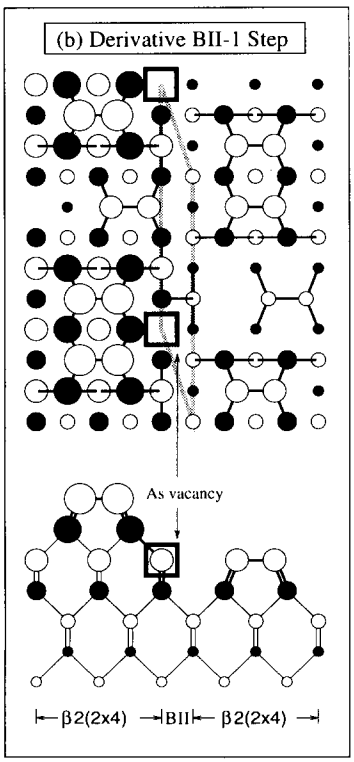

Fig. 5. Top and side views of the derivative (a) BI-1 and (b) BII-1 steps. Details as for Fig. 4.

electron donor as it donates this extra electron. The $Ga^{(2)}$ thus charge compensates four bulk units of the primitive AII Step, as shown in Fig. 4(b), since the latter (as we discussed in Section 3.1) has a deficiency of $0.25e/(1\times)$ electrons. If, on the contrary, the Ga adatom were threefold coordinated through rebonding to the step edge Ga as shown in Fig. 4(a) (AI-1), then the $Ga^{(3)}$ would have to acquire one more electron for the extra bond, instead of giving up one electron. This turns the Ga from a one-electron donor into a one-electron acceptor. From the discussion in Section 3.1, the AI and AII steps have equal amounts but opposite signs of charge. Therefore, a $Ga^{(3)}$ adatom charge compensates four bulk units of the AI step, not the AII step.

(2) *Charge compensation through rebonding.* The example here is the derivative BI-1 step in Fig. 5(a). The parent primitive BI step with a row of $As^{(2)}$ units (Fig. 3(a)) is unstable with respect to rebonding between the $As^{(2)}$ and step edge $As^{(3)}$. Such $As^{(2)}$–$As^{(3)}$ rebonding occurs not only on the BI-1 step but also on flat $\alpha(4\times2)$ surfaces. Unlike Ga, an As atom has deeper p energy levels, making it difficult to promote all but one p electron into the empty energy levels to form the sp electronic configuration required by $As^{(2)}$. There exist, therefore, only $As^{(3)}$ and $As^{(4)}$ motifs on GaAs(001) surfaces, as revealed by the LDA surface calculations [13,14]. This tendency is built into the LCSM calculation by omitting the $As^{(2)}$ motif from our expansion (Fig. 1).

(3) *Charge compensation by native defect.* It is natural to consider native defects as a source for charge compensation as they exist in various charge states. An example here is the BII-1 step (Fig. 5(b)), where, instead of adding atoms, an $As^{(3)}$ vacancy at the step edge of the primitive BII step (see Fig. 3(b)) is created by removal of As. This leaves behind three $Ga^{(3)}$ surrounding the vacant site (denoted by a thick line square), each $Ga^{(3)}$ donating 3/4 electrons from near CBM states to the primitive BII step which is a $0.75e/(1\times)$ electron acceptor (see discussion in Section 3.1). Therefore, a single As vacancy compensates four bulk units of the BII step.

Fig. 6 shows the calculated formation energies of the derivative steps depicted in Figs. 4 and 5. The horizontal axis is the Ga chemical potential which spans an energy range from -0.7 eV to -0.2 eV over which the $\beta2(2\times4)$ surface is stable (see Ref. [14]). We observe from Fig. 6 the following.

(a) Except for a very small region, step formation energies with respect to flat $\beta2(2\times4)$ surfaces are all positive (i.e. endothermic).

(b) The A steps are stabler than the B steps for $\mu_{Ga} > -0.53$ eV. For more negative μ_{Ga} (corresponding to more As-rich conditions), the opposite is true. The

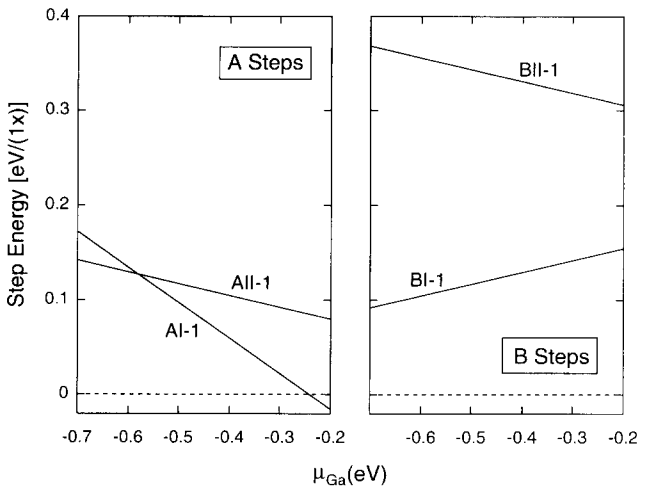

Fig. 6. Step formation energy with respect to the flat $\beta 2(2\times4)$ surface vs. μ_{Ga} for derivative (a) AI-1 and AII-1 and (b) BI-1 and BII-1 steps. The Ga chemical potential μ_{Ga} spans a range from -0.7 eV to -0.2 eV over which the $\beta 2(2\times4)$ surface is stable.

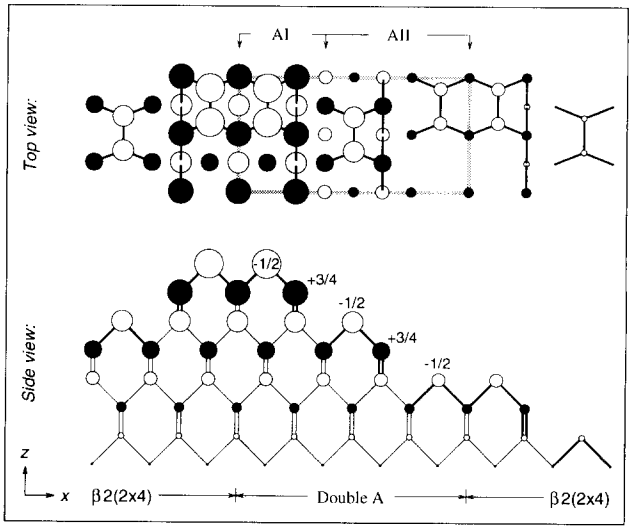

Fig. 7. Top and side views of the double A step. Details as for Fig. 2. Regions corresponding to the AI and AII primitive steps are indicated.

latter conclusion, however, does not hold once interaction between A steps is considered (see Sections 3.3 and 3.4).

(c) The AI-1 step is stabler than the AII-1 step over a large range of μ_{Ga}.

(d) The BI-1 step is stabler than the BII-1 step. The latter is in fact noticeably higher in energy than all three other steps. This can be traced back to step edge $As^{(3)}$ units of the primitive BII step absent on $\beta 2(2\times4)$ surfaces (see Fig. 3(b)).

3.3. Double bilayer steps

Double bilayer steps are composed of two closely packed single bilayer steps of opposite charge and are therefore charge neutral. One example here is the double A step (shown in Fig. 7), made of an AI and AII primitive step pair with the same cell width ($4a_s$) as the $\beta 2(2\times4)$ surface cell. The double A step also has the same surface motifs (i.e. three surface As–As dimers and four sublayer $Ga^{(3)}$ units as the $\beta 2(2\times4)$ surface cell. When the double A step is created from the $\beta 2(2\times4)$ surface, no net change in N_{Ga} takes place. Therefore, according to Eq. (1), only electrostatic interactions contribute to the formation energy of the double A step. We find $\Delta E = 0.05$ eV/(1×1). With respect to the formation of an AI-1 + AII-1 pair, the formation energy of the double A step is given by

$$\Delta E' = 0.09 + 0.5\mu_{Ga} \quad (7)$$

For -0.7 eV$< \mu_{Ga} < -0.2$ eV, over which the flat $\beta 2(2\times4)$ surface is stable, Eq. (7) gives

$$-0.26 \text{ eV/(1×)} < \Delta E' < -0.01 \text{ eV/(1×)} \quad (8)$$

The negative signs in Eq. (8) suggest that, ignoring entropy, formation of the double A step on 2×4 surfaces is favored over the AI-1–AII-1 pair.

3.4. Kink formation

Recently, Heller et al. [5] measured the formation energies of A and B steps via experiments involving thermal excitation of kinks. The idea is that the creation or annihilation of kinks on the edge of a step (S) is always accompanied by the creation or annihilation of step segments of opposite kind to step S. As an example, Fig. 8(a) shows a straight B step whereas Fig. 8(b) shows the same step but with kinks. The formation of the two kinks in Fig. 8(b) not only pushes the center segment of the B step edge towards left but also is followed by the creation of two segments of the A steps (as indicated in Fig. 8(a)). It is important to note that step formation energies measured via kink creation can be qualitatively different from those in Fig. 6 where creation of single steps from flat surfaces is considered. This happens because the kinks enable certain charge compensation between steps, which is forbidden for single and isolated steps. In the example in Fig. 8, the creation of the kinks is equivalent to moving a full 2×4 surface unit (the shaded areas in Fig. 8) from the upper to the lower terrace, with some rearrangement of the surface dimers within the cell. This creates an AI and AII step pair (see the hatched areas in Fig. 8(b)). Despite the noticeable change in surface topology in going from Fig. 8(a) to 8(b), no change in the distribution of surface motifs (and thus, motif related energies) takes place. Also, atoms are transferred in this process

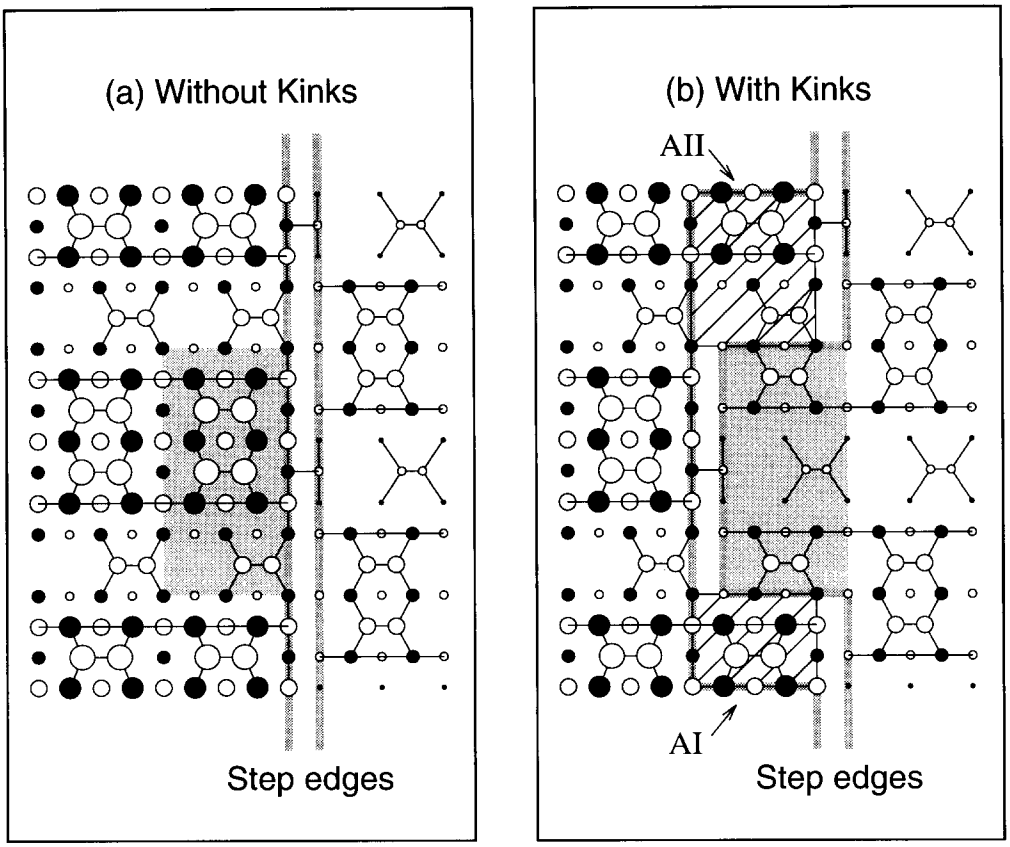

Fig. 8. Top view of (a) a straight and (b) a kinked B step. The filled and open circles are Ga and As respectively, with descending sizes from the surface. The shaded area on the upper terrace in (a) indicates a full 2×4 surface unit which is transferred to the lower terrace (b). The hatched areas in (b) indicate the resulting AI and AII primitive step unit. The thick lines are the upper and lower step edges respectively.

from the surface to bulk GaAs reservoir in units of GaAs molecules (i.e. $N_{Ga}=N_{As}$), thus contributing no net change in N_{Ga}. One can therefore expect that the kink formation energy will be relatively small as it has only an electrostatic component. We obtain $E_{kink}=56$–62 meV per kink which is almost independent of the atomic structures of the B steps (i.e. BI-1, BII-1 etc.). One can keep the kink energy to be purely electrostatic, so long as the (shaded) kink area in Fig. 8(b) is in exact units of the surface 2×4 cells. This observation is in coincidence with the experimental observation [5] that kinks form only in units of 2×4 cells.

We also studied several kink structures on A steps but were unable to find any one in which the B step energy can be significantly lower than those in Fig. 6(b). These results reflect the fact that different from the A steps, complete charge compensation between the two primitive B steps (BI and BII) is absent (see Section 3.1).

4. Discussion

Here, we discuss our theoretical results in light of available experiments. Our discussions include the origin of surface facets, relative stability of A vs. B steps, and the cause for step bunching.

4.1. Origin of surface facets

Both faceting [19] and 2D islanding [7] have been observed on GaAs(001) surfaces. Whether these are caused purely by growth kinetics or also by step energetics remains to be seen. In the work of Ide et al. [7], growth interruption and subsequent annealing were performed on MBE-grown samples with 2×4 surface reconstructions. It was observed that annealing reduces the number of surface islands and greatly smoothes the step shades. Our results (Fig. 6) suggest that steps (thus both 2D islands and surface faceting) are thermodynamically unstable on GaAs(001)-2×4 surfaces.

4.2. Stability of A steps vs. B steps

As mentioned in Section 3.4, Heller et al. [5] have measured step energy by way of measuring the kink distribution on GaAs(001)-2×4. Depending on temperature, they obtained an A step formation energy in the range from 14 to 20 meV/(1×) (these energies include also the corner energies in Ref. [5]). Following Heller et al., one may derive from the calculated kink energy in Section 3.4 the A step formation energy. This gives 28–31 meV/(1×). Heller et al. also determined the B:A energy ratio to be 5.6–6. Ide et al. [7], on the contrary, estimated the ratio from measured anisotropies of equilibrium island shapes. Their value is between 5 to 10. Here, we assume that the A step formation energy is either that of the A step at kinks (up to 28–31 meV/(1×)), or that of the double A step (25 meV/(1×) per single bilayer step), and the B step formation energy is given by the BII-1 step (see Fig. 6) (about 0.1–0.15 eV/(1×)). We then obtain a B:A ratio in the range from 3.2 to 6. Despite the fact that our calculated ratio is in the low end of the experimental values, it indicates clearly that A steps are stabler than B steps.

4.3. Step bunching

Ide et al. [7] recently reported that prolonged annealing (about 20 min) after growth interruption causes step bunching on 2D islands on MBE-grown samples with 2×4 surface reconstruction. The bunching takes place predominantly among the A steps. Ikarash et al. [20] also observed a similar behavior on their MBE samples with also 2×4 surface reconstruction, i.e. step bunching takes place on A steps, but not on B steps. While growth kinetics certainly plays an important role in step bunching, our results on double A steps suggest that bunching may as well be driven by A step energetics, in agreement with the above experimental observations.

Acknowledgments

We would like to thank S. Froyen for many helpful discussions on the subject. This work was supported by the Office of Energy Research (Division of Materials Science of the Office of Basic Science), US Department of Energy, under Contract DE-AC02-83-CH10093.

References

[1] P.M. Petroff, A.C. Gossard and W. Wiegman, *Appl. Phys. Lett., 45* (1984) 620.
[2] A. Gomyo, T. Suzuki, S. Iijima, H. Hotta, H. Fujii, S. Kawata, K. Kobayashi, Y. Ueno and I. Hino, *Jpn. J. Appl. Phys., 27* (1988) L2370.
[3] M.D. Pashley, K.W. Haberen, W. Friday, J.M. Woodall and P.D. Kirchner, *Phys. Rev. Lett., 60* (1988) 2176.
[4] M.D. Johnson, C. Orme, A.W. Hunt, D. Graff, J. Sudijono, L.M. Sander and B.G. Orr, *Phys. Rev. Lett., 72* (1994) 116.
[5] E.J. Heller, Z.Y. Zhang and M.G. Lagally, *Phys. Rev. Lett., 71* (1993) 743.
[6] A. Lorke, K. Pond and P.M. Petroff, *Phys. Rev. B*, in press.
[7] T. Ide, A. Yamashita and T. Mizutani, *Phys. Rev. B, 46* (1992) 1905.
[8] J. Ishizaki, S. Goto, M. Kishda, T. Fukui and H. Hasegawa, *Jpn. J. Appl. Phys., 33* (1994) 721.
[9] G.S. Bales and A. Zangwill, *Phys. Rev. B, 41* (1990) 5500.
[10] E.D. Williams, *Surf. Sci., 299–300* (1994) 502.
[11] P. Smilauer, M.R. Wilby and D.D. Vvedensky, *Phys. Rev. B, 47* (1993) 4119.
[12] T. Ohno, *Phys. Rev. Lett., 70* (1993) 631.
[13] J.E. Northrup and S. Froyen, *Phys. Rev. Lett., 71* (1993) 2276.
[14] J.E. Northrup and S. Froyen, *Phys. Rev. B*, in press.
[15] P. Boguslawski, Q.M. Zhang, Z. Zhang and J. Bernholc, *Phys. Rev. Lett., 72* (1994) 3694.
[16] S.B. Zhang and J.E. Northrup, *Phys. Rev. Lett., 67* (1991) 2339.
[17] M.D. Pashley, *Phys. Rev. B, 40* (1989) 10481.
[18] J.D. Jackson, *Classical Electrodynamics*, Wiley, New York, 2nd edn., 1975.
[19] D.J. Friedman, J.G. Zhu, A.E. Kibbler and J.M. Olson, *Appl. Phys. Lett., 63* (1993) 1774.
[20] N. Ikarash, T. Baba and K. Ishida, *Appl. Phys. Lett., 62* (1993) 1632.